IEEE Access
Multidisciplinary | Rapid Review | Open Access Journal

Received 19 August 2024, accepted 9 September 2024, date of publication 13 September 2024, date of current version 25 September 2024.

Digital Object Identifier 10.1109/ACCESS.2024.3460107

RESEARCH ARTICLE

Improving Pearl Millet Yield Estimation From UAV Imagery in the Semiarid Agroforestry System of Senegal Through Textural Indices and Reflectance Normalization

SERIGNE MANSOUR DIENE[1,2,3], IBRAHIMA DIACK[1,4,5], ALAIN AUDEBERT[2,6], OLIVIER ROUPSARD[3,7,8], LOUISE LEROUX[9,10,11], ABDOUL AZIZ DIOUF[4], MODOU MBAYE[12], ROMAIN FERNANDEZ[2,6], MOUSSA DIALLO[1], AND IDRISSA SARR[1]

[1]Computer Science Department, Cheikh Anta Diop University, Dakar 10700, Senegal
[2]CIRAD, UMR AGAP Institut, 34398 Montpellier, France
[3]LMI IESOL, Centre IRD-ISRA de Bel Air, Dakar 18524, Senegal
[4]Centre de Suivi Ecologique (CSE), Dakar 15532, Senegal
[5]CIRAD UPR AIDA, Dakar 18524, Senegal
[6]UMR AGAP Institut, Univ Montpellier, CIRAD, INRAE, Institut Agro, 34398 Montpellier, France
[7]CIRAD, UMR Eco&Sols, Dakar 34090, Senegal
[8]UMR Eco&Sols, 34090 Montpellier, France
[9]CIRAD, UPR AIDA, Nairobi 00100, Kenya
[10]AIDA, CIRAD, Université Montpellier, 34090 Montpellier, France
[11]International Institute of Tropical Agriculture (IITA), ICIPE Campus, Nairobi 00100, Kenya
[12]ISRA, CERAAS, Thies 3320, Senegal

Corresponding author: Serigne Mansour Diene (smansour.diene@gmail.com)

This work was supported in part by the SustainSahl Project of Europen Union's Horizon 2020 Research and Innovation under Grant 861974; and in part by "Faidherbia-Flux" platform through by Centre de coopération Internationale en Recherche Agronomique pour le Développement (CIRAD), UMR Eco&Sols, Laboratoire mixte international Intensification Ecologique des sols cultivés en Afrique de L'Ouest (LMI IELSOL), Institut Sénégalais de Recherche Agricole (ISRA), CERAAS, and several on-going projects, such as EU-LeapAgri RAMSES II; Agropolis and Total Foundation DSCATT; EU-DESIRA CASSECS; and CIRAD-CRESI-ELISA. The work of Serigne Mansour Diene and Ibrahima Diack was supported by Unmanned Aerial Vehicle (UAV) Equipment through EU-H2020 SustainSAHEL under Grant 861974.

ABSTRACT Enhancing food security in the Sahel through nature-based solutions is urgent given population growth, resource scarcity and climate change. Traditional agroforestry parklands are a farmer- and nature-based widespread form of ecological intensification which randomly integrates trees into crop fields. While most studies estimating crop yields in agroforestry have been conducted in controlled experimental settings, few have addressed the inherent variability in such highly heterogeneous systems. Thus, the purpose of this study is to benefit from a UAV-based proxy-sensing and machine learning approach to address the variability of pearl millet grain yield, according to the distance to randomly distributed trees in a traditional agroforestry system dominated by *Faidherbia albida* (i.e. groundnut basin of Senegal). 21 vegetation indices (VIs), 32 normalized difference texture indices (NDTIs) derived from multispectral drone images, and normalization variables for radiative conditions were used with yield data collected in 15 plots (around 1 ha each) and subplots (15 m^2 each) displayed at 3 distances from the tree over five cropping seasons (2018–2022). In this context, the optimal phenological stage was determined for predicting pearl millet grain yield, which proved to be the pre-heading period. This period was used as the basis for our machine learning model training dataset in the subplots. Two models, Random Forest (RF) and Gradient Boosting Machine (GBM) were compared by combining VIs, NDTIs and normalization variables. GBM was the best-performing model, explaining 78% of observed pearl millet yield variability over five years in the subplots, with a RMSE of 16 g.m^{-2}. This study revealed that NDTIs calculated from red and green bands were more

The associate editor coordinating the review of this manuscript and approving it for publication was Yang Tang.

influential for yield estimation than those based on near-infrared. These results were subsequently used to predict yield in all plots, resulting in a mean relative error of 17.5% between yields estimated by the farmers and GBM-estimated yields. This approach represents a pathway to assessing the withinfield yield variability in highly heterogeneous agroforestry plots and to demonstrate, quantify and optimize tree benefits for ecological intensification.

INDEX TERMS Agroforestry, drone, heterogeneity, multispectral, machine learning, upscaling, yield.

I. INTRODUCTION

One in nine people in the world is undernourished, and the most recent evidence available suggests that the number of people unable to afford a healthy diet around the world has increased by 112 million to almost 3.1 billion, reflecting the impacts of rising consumer food prices during the pandemic [1]. In 2020, the African population was approximately 1.312 billion, accounting for approximately 17% of the global population [2]. This population increase has consequences such as a reduction in arable land, which requires mechanisms to eliminate hunger, ensure food security, improve nutrition, and promote sustainable agriculture, as outlined in Sustainable Development Goal 2 [3]. Indeed, at a global scale, the paradigm has shifted from simple agricultural intensification to ecologically intensive agricultural practices [4], aiming to increase yields while limiting the environmental impacts of agricultural systems. These challenges are particularly critical in Sub-Saharan Africa, where smallholder family farming serves as a local source of food and income and contributes significantly to overall food and nutrition security [5]. Moreover, Sub-Saharan Africa is one of the regions in the world where agriculture is particularly constrained, with observed yields well below potential yields [6]. Agroforestry, the combination of trees, crops, and livestock in the same area [7], has been recognized as a mechanism to increase resilience against land degradation and climate change [2]. The adoption of agroforestry depends on many management goals, drivers, and contextual factors [7]. In most cases, assets related to ecosystem services and food security are the main motivating factors in agroforestry adoption [8], [9]. Agroforestry also has supportive functions, for example, soil fertility improvement or water recycling [10], [11], [12], particularly when management techniques such as mulching or conservation agriculture are applied [13]. agroforestry is therefore often considered a way to sustainably intensify farming practices for enhanced food security using socially and cost-effectively managed techniques [7]. Many agroforestry options achieve this through low external input requirements, high recycling rates, and crop-livestock integration [14]. In addition, agroforestry provides attractive alternatives to monoculture, especially when the benefits of association can be quantified and explained convincingly based on phenomena such as extended resource acquisition, complementarity, and facilitation [12]. Consequently, the aim of this study is to optimize crop yields in agroforestry context. The study site here is a Faidherbia albida parkland located in the groundnut basin of Senegal. Faidherbia albida is the main tree species of the parkland (38% of the trees) [15]. However, the presence of trees in the plots creates a complex configuration within the field, unlike in experimental agroforestry plots. The trees contribute to significant spatial heterogeneity in crop yield, leading to both spatial and temporal variability, compounded by different agricultural practices among farmers and across years. Moreover, yield assessment is primarily conducted under controlled experimental conditions using costly and non-scalable manual methods. Therefore, the utilization of new technologies emerges as a critical tool for evaluating crop yields. Remote sensing and proxy detection are attractive tools for the mapping of crop traits. As one example, the estimation of yields of cereal crops in a complex agricultural landscape was made possible by the democratization of satellite imagery of high spatial-temporal resolution (VHR: e.g., Sentinel-2, Landsat 8, or PlanetScope). Such tools with high spatial resolutions of 10 m and 3 m have demonstrated their performance in estimating crop yield [16] and ecosystem service relationships [17] at the landscape scale. However, Sub-Saharan Africa and specifically the groundnut basin of Senegal are characterized by relatively small plots, different agricultural practices, environmental heterogeneity (caused by the local impact of trees), and cloud cover during pearl millet growth stages. Such characteristics significantly limit the application of satellite images, especially at the intra-plot scale. Recent technological advancements in unmanned aerial vehicles (UAVs) and sensor miniaturization have created interesting prospects in crop characterization. UAVs are widely used for intensive monitoring of cultivated fields. They offer the opportunity to capture intra-plot variability and plot yield heterogeneity. Vegetation indices derived from multispectral and visible images show sensitivity to crop development stage and canopy structure. Through the use of UAVs, high-resolution spatiotemporal remote sensing data for crop monitoring can be acquired for various applications [18], [19], [20], including agroforestry [21]. UAV sensors can be used to detect crop-related diseases [22], analyze crop development [23], and assess plant water status [24]. Aerial images from multispectral and hyperspectral cameras have greatly contributed to crop evaluation and the estimation of biophysical parameters using vegetation indices [25]. Reference [26] estimated rice grain yield at different developmental stages and compared indices based on visible and multispectral

imagery, with the VARI (visible atmospherically resistant index) for color-based indices and the NDVI (normalized difference vegetation index) for spectral-based indices being the best predictors. Several studies have utilized color indices such as the normalized green–red difference index (NGRDI), vegetative index (VEG), and primarily the excess green index (ExGI) calculated from RGB bands to map vegetation cover fractions and estimate biophysical parameters [27], [28], [29]. In addition, recent studies have tested the potential of texture indices based on the gray-level cooccurrence matrix (GLCM) for estimating rice aboveground biomass or monitoring wheat fusarium head blight in combination with vegetation indices derived from visible or multispectral images [30], [31]. Reference [32] combined vegetation indices with texture indices into the normalized difference texture index (NDTI) to estimate rice grain yield using a hyperspectral camera. Texture analysis combined with vegetation indices improved the prediction of rice leaf area [33]. NDTIs generated new perspectives for further improving the prediction of crop performance in general, particularly crop yield [34]. Textural analysis pertains to the spatial variation of grayscale levels in an image. Hence, integrating texture features into yield estimation models could deepen our comprehension of spatial variations that might influence crop productivity. The utilization of NDTIs combined with texture indices, facilitates the incorporation of textural variations for a more effective capture of the signal characteristic. In one only of the fields surveyed by the present study, [35] used a MS camera and flew an UAV at the time of harvest to compare measured and sensed pearl millet yield. Although this pioneering study was promising, the developed approach, with a R2 of 0.47 and a RMSE of 46%, needed to be improved using more data. The considered options to improve its performance are: (i) to repeat the study for several years and over a larger network of plots in order to test the robustness, (ii) to implement multiple flights throughout the growing season to determine the optimal phenological period for yield estimation, (iii) to combine several VIs and texture indices into machine learning approaches. However, flying at different dates and times causes biophysical conditions to vary, such as global radiation, diffused fraction and sun angle. Therefore, standardizing radiative conditions between flights becomes advisable. The aims of this study were to build a generic model on a large network of plots and years for estimating pearl millet grain yield in a heterogeneous landscape and specifically to (i) assess the best period for millet grain yield prediction; (ii) assess the potential of texture indices for improving the estimation model and standardization variables for normalizing reflectance; and (iii) determine upscale productivity from small sampling plots to the whole stand.

II. MATERIALS AND METHODS

A. STUDY SITE

The study was carried out in the agroecological zone of the groundnut basin of Senegal, more precisely around the village of Sob in the commune of Niakhar located in the Fatick region (Fig. 1). The climate is Sudano-Sahelian. According to [36], rainfall decreased from 900 to 400 mm between 1950 and 1995 (the driest period) and then recovered partially to ca. 500 mm by 2015, although with large interannual variability in its amount and distribution. The area is characterized by one rainy season that usually lasts from July to October, with heavier rainfall recorded between August and September. Small family farming, with low uses of external inputs, is the main source of food and income. The area is characterized by a tree-based cropping system, also known as parkland, where trees are combined with crops. A highly instrumented site called ''Faidherbia-Flux'' (https://lped.info/wikiObsSN/?Faidherbia-Flux); registered in FLUXNET as 'SN-Nkr';) was launched in 2018 in the area (see Fig. 1). Faidherbia-Flux is located at 14°29′44.916″N and 16°27′12.851″W and has instruments and facilities for monitoring micrometeorology, soil moisture, the NDVI, surface temperatures, crop productivity, and yields, among other parameters. A standard meteorological station was available at the flux tower. The soil profile sampled during this study indicated a loamy sand texture with homogeneous sand fractions along the profile; clay fraction and bulk density variations were found at depth intervals of 0-50, 50-100, and 100-200 cm [37]. The cropping system was an annual rotation between pearl millet and groundnut under-crops below Faidherbia. Pearl millet (Pennisetum glaucum, L.), the crop being researched in the current study, is a foundation of food security in rural areas, with consumption increasing by 50% during the lean period [38]. It is the sixth cereal [39] in terms of world production and is considered a ''cereal of last resort'' for farmers in especially challenging arid conditions [40].

B. FIELD DATA COLLECTION AND SUBPLOT ARRANGEMENT

From 2018 to 2022, a total of 16 fields of ca. 1 ha cultivated by millet were monitored during the cropping season. We measured the pearl millet grain yield of each of the subplots from each plot at harvest. The ears (part of a millet plant that bears the grains) were weighed to determine fresh weights in the field with precise scales to the nearest gram. The ears were then air dried and sent to the laboratory for oven drying at 65°C until constant weight and then weighed. In each plot, we selected an average of 4 *F. albida* trees. For each tree, subplots with an area of 15 m^2 were displayed at three distances, following [35]: at the edge of the tree crown (to ensure the strong impact of the neighbor tree on crop growth with still visibility of the subplot during UAV flights), at 2.5 times the crown radius (R) and 5 R (see Fig. 2). In 2018, 2020 and 2022, plot ''0'' was also harvested completely by the farmer, and in 2019, plot ''8'' was harvested as well; ears were bundled, bundles were counted and weighed, and the ratio between the fresh weight of the ears and the dry weight of the grains obtained in

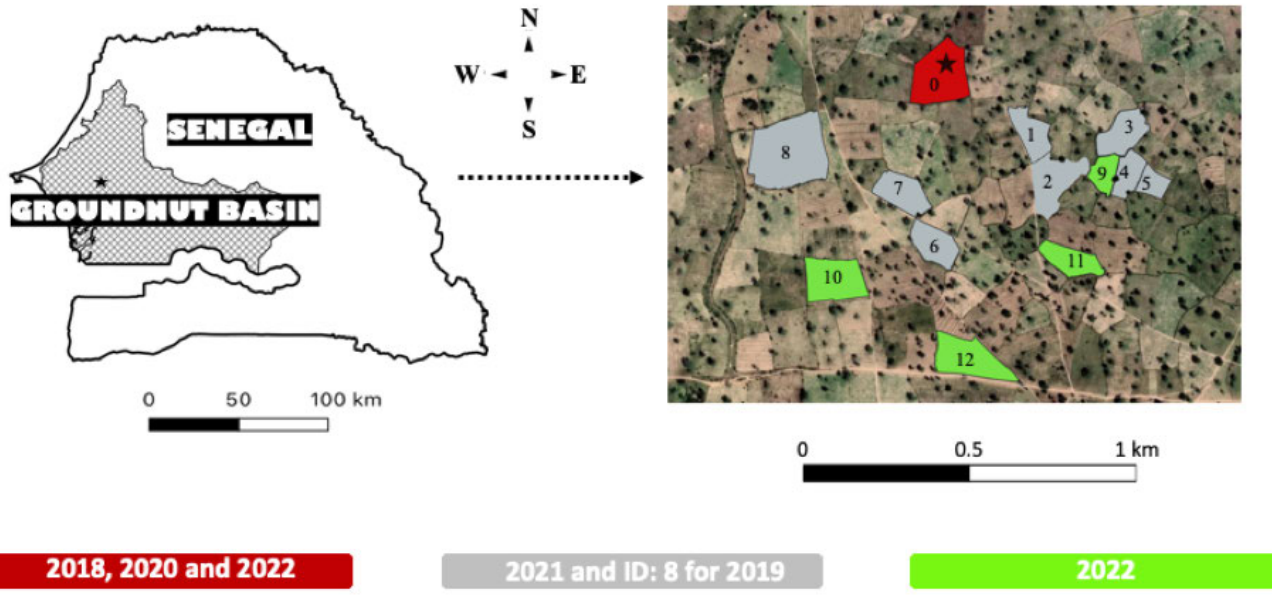

FIGURE 1. Location of the study area in the groundnut basin of Senegal with the position and IDs of different plots monitored from 2018 to 2022. The star corresponds to the position of the flux tower. Image source: Google Satellite ©* background, 2022.

TABLE 1. Yields data and standardized variables from 2018 to 2022.

Variables	Count	Mean	Std	Min	Max
Air relative humidity (%)	158	72.46	10.28	61.07	95.90
Soil surface temperature (C)	158	34.03	4.09	26.12	42.66
Photosynthetically active radiation (micromolephoton. $m^{-2}s^{-1}$)	158	1344.61	611.37	46.31	2116.00
Solar azimuth (rad)	158	4.18	1.32	1.35	5.10
Millet grain yield (g.m^{-2})	158	79.91	33.08	4.99	166.48

TABLE 2. Basic parameters for the two multispectral cameras.

Sensor	Wavelength (nm)	Pixels size	Flying heigt (m)	Resolution (cm)
AIRPHEN	450, 530, 560, 675, 730, 850	1280 x 980	50	2.7
DJI Mulitispectral	450, 560, 650, 730, 840	1600 x 1300	25 50	1.3 2.7

the laboratory from subplot samples was applied to infer the whole plot ear dry mass yield. The relative yield error (RYE) was computed as Eq. 1, hence assuming that the measurement error can be larger than the simulation error due to the high difficulty and assumptions related to the yield measurement at the whole-plot scale. Field data were aggregated into a ground truth database comprising of 158 subplots from 5 years and 16 plots (Table 1).

$$RYE = \frac{|(Ymeas - Ysim)|}{Ysim} \quad (1)$$

RYE = relative yield error, Ymeas = real yeald mesurement and Ysim = simulated yeald. |(Ymeas - Ysim)| represente absolute value of the diferent betwen Ymeas and Ysim.

C. IMAGE ACQUISITION AND PREPROCESSING

In this study, we used two different UAVs. Details about the differences between the two drones are shown in Table 2. From 2018 to 2020, a FeHexaCopter V2 UAV (Mikrokopter - HiSystems GmbH, Moormerland, Germany) [41] was used with two onboard cameras mounted on a two-axis gimbal. The first camera was a visible RGB ILCE-6000 (Sony Corporation, New York, USA). The second camera was an AIRPHEN multispectral camera [42] with a focal length of 08 mm. The AIRPHEN camera had six wavelengths centered at 450, 530, 560, 675, 730, and 850 nm with a spectral resolution of 10 nm. In this study, we discarded the 530 nm wavelength because it was unavailable with the second drone's camera. The drone flights were carried out at an altitude of 50 m (due to the 30 m high flux tower) with a longitudinal overlap rate of 80% and lateral overlap rate of 70%. From 2021 to 2022, the study was conducted with a DJI Phantom 4 Multispectral multirotor drone [43]. The Phantom 4 Multispectral has a payload capacity of 400 g and a maximum range of 5000 m. The drone's flight time varied between 12 and 22 minutes depending on the battery's level and weather conditions. The UAV was equipped with a digital camera that measured in the visible band and 5 spectral bands centered at 450, 560, 650, 730, and 840 nm with a spectral resolution of 16 nm. Drone flights were carried out in open-sky conditions and low wind speeds between 12 and 16 h local time. This trade-off was to minimize shade over the plot, cover several plots on the same day, and avoid windy periods. The DJI Gs Pro application was used to define the flight missions. Camera parameters were adjusted based on sunlight exposure. Images were captured every 2 seconds with a longitudinal overlap rate of 80% and a lateral overlap rate of 70%. Flight altitudes were fixed at 25 m, except over the flux tower plot, and we obtained a spatial resolution of 1.3 cm. Details of image acquisitions are shown in Table 3.

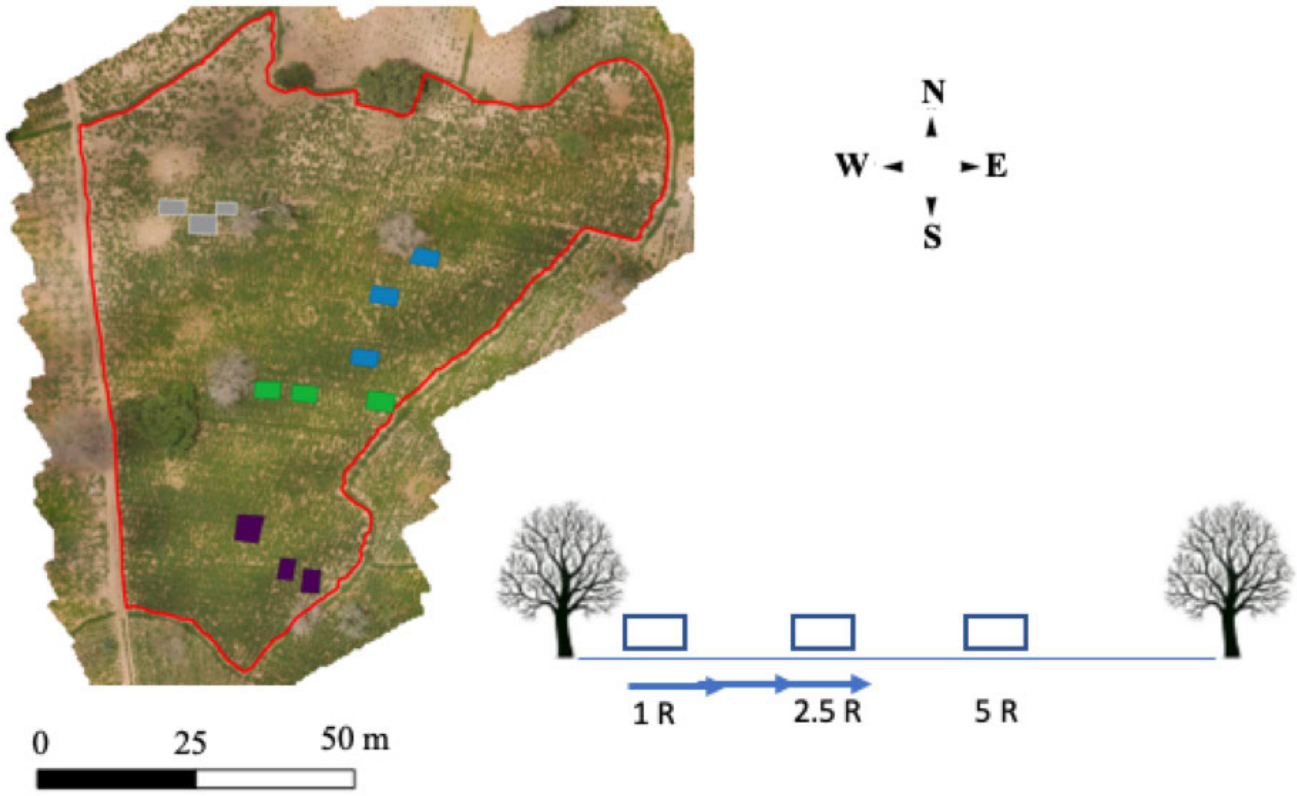

FIGURE 2. One plot example of pearl millet crop sampling at three distances from 4 *F. albida* trees (gray crown (unleafed during the wet season), 4 colors of subplots). We compared three distances to the tree: at the edge of the tree crown (1 R), at 2.5 radii (2.5 R), and at 5 radii (5R), where R is the radius of the tree crown. Total number of subplots per plot = 12.

TABLE 3. Acquisition of multispectral (Ms) images for 5 years of experiments, according to pearl millet growth stages. N = 16 orthomosaic. In red, years in which the entire plot was harvested (ID: 0 for 2022).

Sensors	Experiment	Plots (IDs)	Ms images	
			Acquistion date	Growth stage
AIRPHEN	2018	0	2018-08-30	Post-heading
	2018	0	2018-10-08	Harvest
	2019	8	2019-09-05	Post-heading
	2019	8	2019-10-17	Harvest
	2020	0	2020-09-04	Post-heading
	2020	0	2020-10-07	Harvest
DJI Multispectral	2021	1 to 8	2021-08-05	Pre-heading
			2021-08-15	Pre-heading
			2021-09-04	Post-heading
			2021-09-14	Post-heading
			2021-10-08	Harvest
	2022	0 and 9 to 12	2022-08-15	Pre-heading
			2022-09-04	Post-heading
			2022-10-04	Harvest

1) ORTHOPHOTO-MOSAIC GENERATION AND CO-REGISTRATION

The orthophotos were obtained from UAV photography combined with a 3D model. Photogrammetric techniques were used to reconstruct artificial and natural elements on a plane from pairs of images with a common part determined by the overlap rate defined during the flight mission execution. An automatic image processing pipeline was designed to generate multispectral orthophotos [44] using a digital elevation model at 5 wavelengths using Agisoft Metashape Python API (Metashape Professional 1.7.4, Agisoft LLC, Russia). Co-registration is a process that aligns multiple images from different sources and times so that they can be compared and overlaid accurately. We then performed a geometric correction to co-align the orthophotos, using the harvest date orthophoto as a reference for each plot. The co-registration algorithm was performed using the rgdal [45] and raster [46] packages in R software version 4.2.2 [47].

2) VEGETATION INDEX CALCULATION

A literature review was conducted to select vegetation indices based on spectral wavelengths and others derived from the three channels of RGB cameras, which were used for vegetation monitoring and yield estimation. These indices were employed to establish a statistical model correlating 21 vegetation indices (Table 4) with millet yield, aiming to pinpoint the most predictive ones. Every single index was averaged on all pixels of each subplot.

3) TEXTURAL INDEX CALCULATION

Recent studies [30] and [31] have shown the potential of texture indices derived from UAV imagery to improve the

TABLE 4. List of the 21 vegetation indices used in this study.

	Index	Formula	Source
Spectral indices	NDVI	$\frac{Nir-Red}{Nir+Red}$	[48]
	Ci_Green	$\frac{Nir}{Green}-1$	[49]
	Ci_redEdge	$\frac{Nir}{RedEdge}-1$	[49]
	DVI	$Nir-Red$	[50]
	NDRE	$\frac{Nir-RedEdge}{Nir+RedEdge}$	[51]
	SR	$\frac{Nir}{Red}$	[52]
	GNDVI	$\frac{Nir-Green}{Nir+Green}$	[53]
	SAVI	$\frac{Nir-1.5\times Red}{Nir+Red+0.5}$	[54]
	TVI	$\sqrt{NDVI}+0.5$	[48]
	CTVI	$\left(\frac{NDVI+0.5}{\lvert NDVI+0.5\rvert}\right)\times\sqrt{\lvert NDVI+0.5\rvert}$	[55]
	OSAVI	$\frac{Nir-Red}{Nir+Red+0.16}$	[56]
Color indices	MGRVI	$\frac{Green^2-red^2}{Green^2+red^2}$	[57]
	GLA	$\frac{2\times Green-Red-Blue}{2\times Green+Red+Blue}$	[58]
	NGDRI	$\frac{Green-Red}{Green+Red}$	[59]
	NDBRI	$\frac{Red-Blue}{Red+Blue}$	[60]
	NDBGI	$\frac{Green-Blue}{Green+Blue}$	[61]
	NDGRI	$\frac{Red-Green}{Red+Green}$	[62]
	ExGI	$\frac{2\times Green-Red-Blue}{Red+Blue+Green}$	[63]
	RGBVI	$\frac{Green^2-(Red\times Blue)}{Green^2+(Red\times Blue)}$	[57]
	RB	$\frac{Red}{Blue}$	[64]
	VARI	$\frac{Green-Red}{Green+Red-Blue}$	[65]

monitoring of wheat ears and the estimation of aerial biomass. Thus, we used the gray level cooccurrence matrix (GLCM) [66] to calculate eight texture properties based on the GLCM (Fig. 3), namely, mean (MEA), variance (VAR), homogeneity (HOM), contrast (CONT), dissimilarity (DISS), entropy (ENT), second-moment (SM), and correlation (COR). These texture measurements were calculated using R and the glcm package [67]. We used the smallest window size (3×3 pixels) and all directions to perform texture analysis. The analysis was performed with the green, red, and near-infrared bands of the multispectral imagery.

4) COMPUTATION OF NORMALIZED DIFFERENCE TEXTURE INDEX (NDTI)

Following [31], the traditional definition of the normalized difference vegetation index (NDVI) was used as a reference to calculate the normalized difference texture index (NDTI) [33] (Eq. 2). The NDTI differs from the NDVI in its calculation procedure, as it is computed based on different combinations of selected bands (green, red, and near-infrared) during the calculation of statistical texture properties from the gray-level co-occurrence matrix. Only the NDTIs were subsequently used to improve millet grain yield estimation.

$$NDTI_{Tiab} = \frac{T_{ia} - T_{ib}}{T_{ia} + T_{ib}} \tag{2}$$

where T_i is a texture index (with i ranging from 1 to 8, according to Fig. 3), and a and b are random spectral bands.

5) STANDARDIZATION VARIABLES

In the context of this study, the UAV monitoring of a network of smallholder farms involved capturing images at different times and days due to battery limitations and in situ ground truth measurements. Each drone flight was carried out under varying environmental conditions, and the radiometric calibration of the numerical values of the different spectral bands was a normalization solution, as in [31]. However, in this study, reference carpets were available only from 2018 to 2020 when using the AIRPHEN camera. Due to slight differences in drones, bands, resolution, time of flight, and availability of reference carpet, we introduced a standardization step. We tested a few meteorological variables that were measured or computed by standard weather stations and that were likely to affect the signal, and we finally selected the most predictive ones, i.e., the relative humidity of the air (measured by CS615, Campbell Scientific), the surface soil temperature (by Type-T thermocouples), the photosynthetically active radiation (PAR, by SKP 215, Skye instruments; NB: the global radiation is available in many weather stations instead of PAR, but both variables are extremely well correlated) and the solar azimuth (computed from coordinates and time using a standard astronomical model). The purpose was not to introduce field covariables in the model to explain yield variability but rather to standardize the signal between days and hours of flights to dampen noise in reflectance. These variables were available at the meteorological station of the flux tower antenna at the semi-hourly time-step since 2018. Hence, for each image, we used the standardization variables acquired at the exact date and time of the flight (Table 1).

D. MODEL CALIBRATION AND VALIDATION

The overall approach for developing the models of prediction of millet grain yield for different variables is given in Fig. 4. In this study, we refined the models in sequence. First, we tested the potential of vegetation indices (Vi) in predicting only millet grain yield. Second, we assessed the impact of the NDTI on the prediction by combining vegetation and texture indices. Finally, we added standardization variables to account for changes in the environment during image acquisition and to normalize the wavelength reflectance. At each step, we selected the best variable combination.

1) SELECTION OF THE BEST ACQUISITION DATE FOR MILLET GRAIN YIELD ESTIMATES

The UAV allowed for regular monitoring of the cultivated plots from the development stage to the maturation of millet. We sought to determine the best date that predicted millet grain yield most accurately. For this exercise, we first discarded years when UAV flights were not carried out over the entire crop cycle (2018 to 2020). Following this, to determine the optimal correlation date for the years 2021 and 2022, we performed a simple linear regression between the same vegetation index and yield for these two

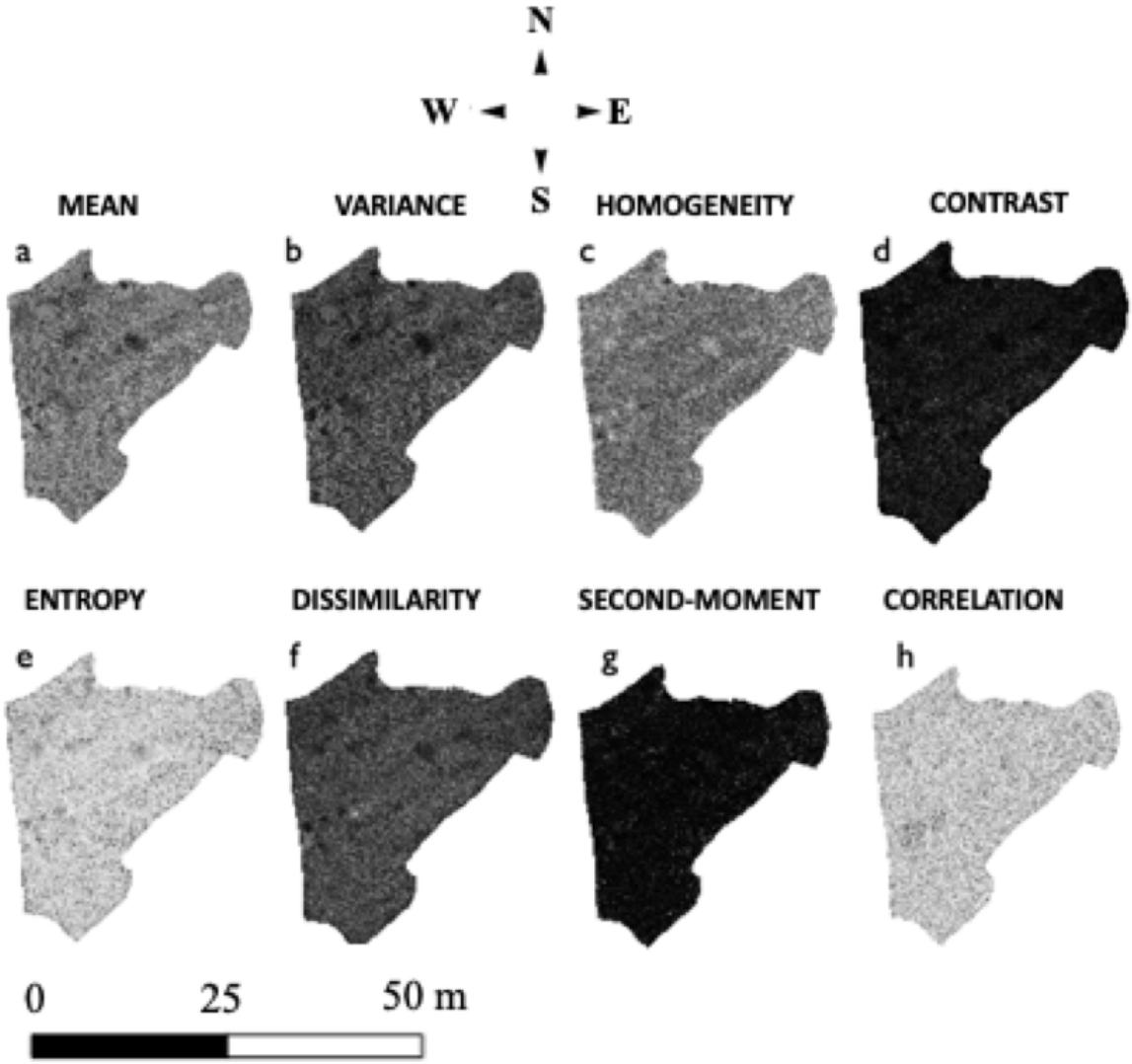

FIGURE 3. Eight GLCM-based texture measurements of Near Infrared band for one example plot, in 2021.

years. Considering the availability of 21 vegetation indices, and recognizing that the correlation between these indices and yield varies based on the index and date, NDRE was chosen from the 21 indices. This choice was made due to its sensitivity to crop growth, allowing us to evaluate its correlation with millet grain yield and to conduct a comparative analysis.

2) DATA PREPROCESSING

Using UAVs can lead to errors that are related to weather conditions, terrain geometry, etc. Field measurements ('ground truth' here) can also have errors related to inaccurate note-taking or incorrect manipulation. Preprocessing of the data is fundamental to obtain reliable and reproducible results. We first discarded outlier data for millet grain yield values using the interquartile range technique [68], [69]. Then, we evaluated the performance of different variables to select the most relevant variables for predicting millet grain yield. This selection was made using a recursive feature elimination (RFE) algorithm [70], [71]. The algorithm was based on the machine learning model used for prediction and performed a 5-fold cross-validation. Additionally, we conducted an analysis to detect variables exhibiting collinearity or strong dependence. This analysis was critical to avoid overfitting the model. We used the variance inflation factor (VIF) to select collinear variables for elimination [72]. VIF [71] (Eq. 3) uses simple linear regression between the different input variables of the model to calculate the Pearson correlation coefficient [73] and gradually eliminate collinear variables. Elimination was performed using a VIF < 2 [74] to exclude collinear variables and retain the variables that would be used in the final models (Fig. 5).

$$VIF_i = \frac{1}{1 - R_i^2} \tag{3}$$

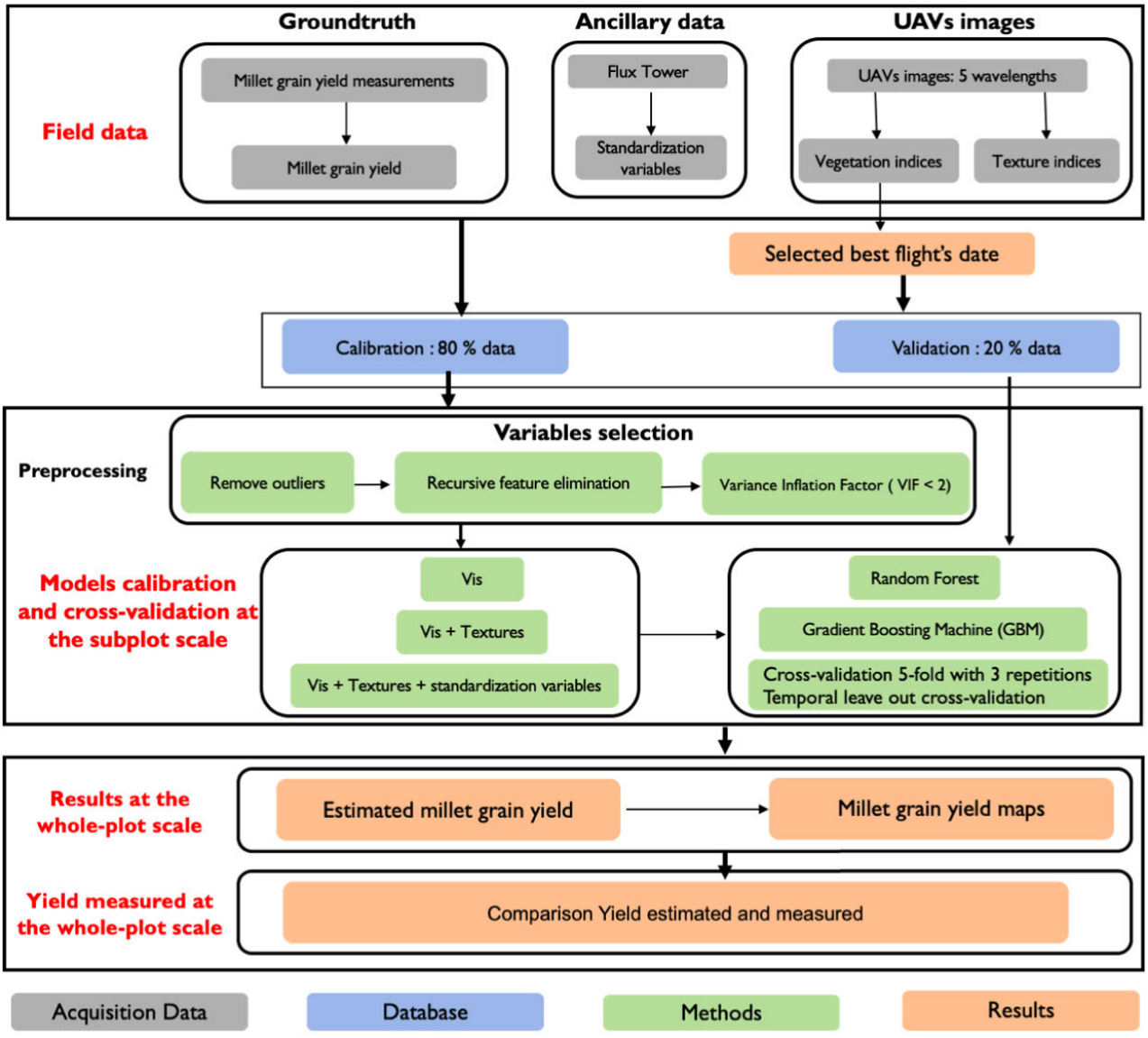

FIGURE 4. Schematic description of the workflow for pearl-millet grain yield estimation.

where VIF_i stands for the variable inflation factor of the variable i and R_i^2 stands for unadjusted coefficient of determination for regressing the i^{th} independent variable on the remaining ones.

3) RANDOM FOREST

Random forest (RF) [75] is a widely used machine learning method for predicting continuous variables using multiple random decision trees and other optimization parameters. For the latter, we used the number of decision trees (n_estimators), maximum depth of each tree (max_depth), minimum number of samples (min_samples_leaf), and random number generator (random_state). Hyperparameter optimization was performed using a 5-fold cross-validation grid search that tested all possible combinations of parameters. We then performed 5 iterations on the grid search to select the best combination based on the lowest mean squared error (MSE). The RF model takes as input only the selected remote sensing and microclimatic variables (Vi, combination of Vi + NDTIs, and combination of Vi + NDTIs + standardization variables) obtained through RFE and VIF and relates them to millet grain yield. The grid search result for the Vis + NDTIs + standardization variables model yielded 500 for n_estimators, 15 for max_depth, 2 for min_samples_leaf, 70 for random_state and True for oob_score.

4) GRADIENT BOOSTING MACHINE

As with the RF, we applied a grid search with 5-fold cross-validation. The hyperparameters used to optimize the gradient boosting machine (GBM) method were the

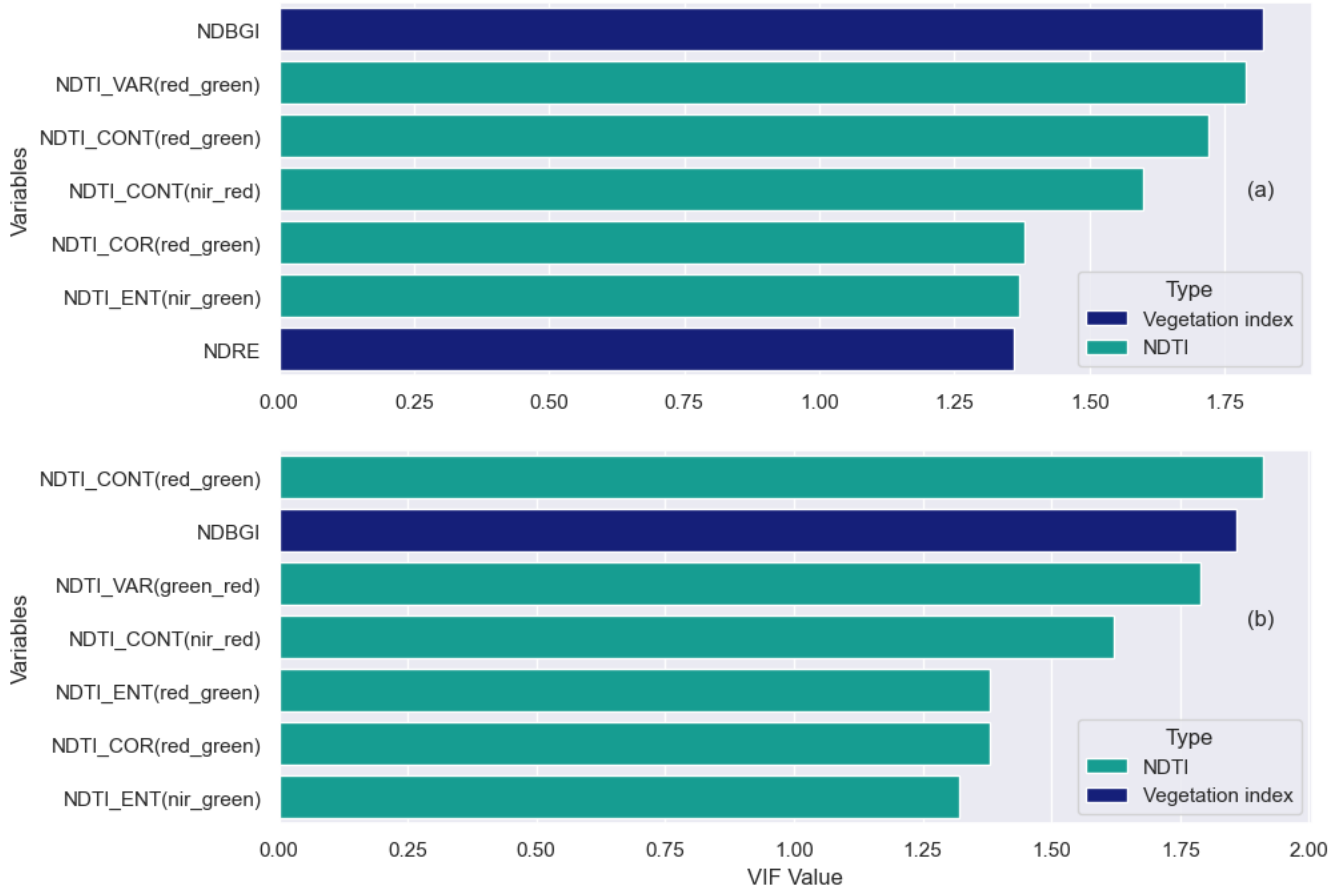

FIGURE 5. Selected explanatory variables after performance and collinearity tests. (a) presents the selected variables for the GBM model, while (b) showcases the selected variables for the RF model.

same as those for RF, with learning_rate as an additional parameter. The model for the combination of Vi + NDTIs + standardization variables, which produced the lowest RMSE, was obtained using the following values: learning_rate (0.002), max_depth (15), min_samples_leaf (2), n_estimators (1000), and random_state (10).

E. ASSESSMENT OF MODEL PERFORMANCE

To evaluate the quality of the millet grain yield estimation models, we split the dataset into 80% training data and 20% external validation data. We used the coefficient of determination R^2, root mean squared error (RMSE), and relative root mean squared error (RRMSE) as metrics to select the best machine learning model between RF and GBM (for the different variable combinations) based on the external validation results. We also performed 5-fold cross-validation with 3 repetitions on the training data. To mitigate biases stemming from temporal autocorrelation, we conducted temporal leave-out cross-validation to assess the robustness of the machine learning models. The temporal cross-validation process involved training the model using data from four years (e.g., 2018, 2019, 2020, and 2021) and validating in the remaining year (e.g. 2022). This procedure was iterated to calculate the RMSE for validation across all years. The assessment of feature importance was conducted using the SHAP value method, which proves instrumental in offering intricate interpretations of variables by delineating the impact of each variable's contribution on the model. Additionally, satellite images from Landsat 8, downloaded via the Google Earth Engine platform, were employed to construct a millet grain yield estimation model with a view to comparing it with the results obtained by UAV. In 2020, [17] demonstrated that GCVI around the pearl millet flowering period is a good estimator of yields. Thus, we relied on this result to calculate the Green Chlorophyll Vegetation Index (GCVI) of different plots monitored from 2018 to 2022 using Landsat 8 satellite imagery. The spectral bands of Landsat 8 were resampled to a spatial resolution of 15 meters using the panchromatic band and the pansharpening technique. The resulting yield models facilitated the assessment of the robustness and relevance of using UAV-acquired data, which possess very high spatial resolution.

F. MAPPING OF THE MILLET GRAIN YIELD

The scaling-up from subplot to whole-plot yield was carried out on 4 plots where the entire grain yield of the plot was

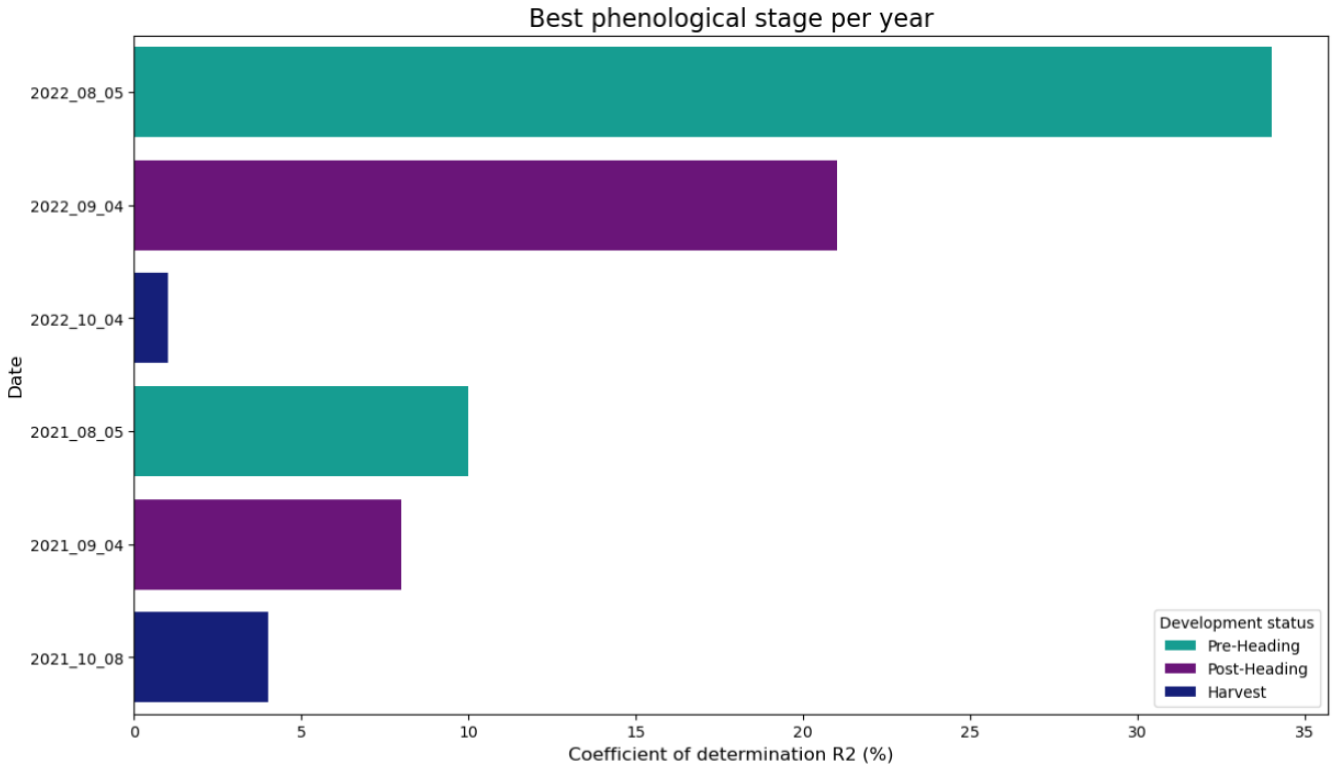

FIGURE 6. Correlation between NDRE and millet grain yield for each date during the millet cycle.

harvested (Table 3). The most performant machine learning model (based on data from the 16 plots, 5 years and the best date of acquisition for each) among different variable combinations was used to produce grain yield maps for the latter plots. All trees (*F. albida* and other species) and equipment present on the different plots were masked to avoid misinterpretation of the spatial model. Thus, we compared the yield estimated from the final model with the yield actually measured in the field. The total millet grain yield of the plot was calculated by normalizing the sum of yield values with the total number of pixels in the plot.

III. RESULTS

A. SELECTION OF THE BEST UAV FLIGHT DATE

The intensive monitoring of millet's developmental stages allowed us to analyze the relationship between VIs (NDRE in this part) and millet grain yield for each image acquisition date per year where several dates of flights were available (2021 and 2022). For both years, we encountered the same ranking of dates, with the pre-heading date presenting the best coefficient of determination (see Fig. 5). However, we found large discrepancies in the R^2 values between 2022 and 2021, with better correlations between the NDRE and millet grain yield in 2022 (pre-heading: $R^2 = 0.34$, harvest: $R^2 = 0.01$) than in 2021 (pre-heading: $R^2 = 0.10$, harvest: $R^2 = 0.04$). Indeed, the study was conducted on a large network of 12 smallholder plots (2021 and 2022), where pearl millet was usually mixed with weeds, leading to the saturation of VIs, in addition to the inherent differences caused by agricultural practices and environmental factors. Due to this inherent variability and the absence of other cycle periods in previous years, it was preferred not to use a single date across years (such as the pre-heading date); rather, it is better to rely on the best date for each year and each plot.

B. BEST MODEL FOR ESTIMATION OF MILLET GRAIN YIELD

We used machine learning methods (RF and GBM) with various combinations input variables (VIs, NDTIs, standardization variables) to evaluate the contribution of NDTIs and standardization of reflectances in estimating millet grain yield. The best combinations of features were to add them all, i.e., VIs + NDTIs + standardization variables (Table 5). We based our selection of the best combination of variables (the feature importance is shown in Fig. 7(a) for GBM method and 7(b) calculated with the Out-Of-Bag (OOB) of the RF method) for different machine learning methods on R^2, RMSE, and RRMSE using external validation. Ultimately, the GBM produced a cross-validation CV_R^2 of 0.71 and a CV_RMSE of 19 g.m^{-2} on 80% of the training data (see Fig. 8(a)). For external validation (see Fig. 8(b)) on the remaining 20% of the test data, the GBM yielded an R^2 of 0.78, an RMSE of 16 g.m^{-2}, and an RRMSE of

TABLE 5. Summary of calibration and validation results.

		Calibration					Validation		
Model	Variables	R^2	RMSE (g.m^{-2})	RRMSE (%)	Cross_Val R^2	Cross_Val RMSE (g.m^{-2})	R^2	RMSE (g.m^{-2})	RRMSE (%)
RF	Vis	0.79	16	20	0.69	21.21	0.48	24	34
	Vis + NDTIs	0.87	13	16	0.74	19	0.60	21	30
	Vis + NDTIs + standardization variables	0.88	12	15	0.71	19	0.64	20	28
GBM	Vis	0.95	08	09	0.67	20	0.29	28	39
	Vis + NDTIs	0.94	09	10	0.76	18	0.64	20	28
	Vis + NDTIs + standardization variables	0.95	08	10	0.71	19	0.78	16	22

TABLE 6. Model performance with temporal leave-out cross-validation. The year specified in the "year" column corresponds to the year used for validation.

	Year	RF	GBM
		RMSE (g.m^{-2})	
80-20 (train-test) validation	2018 - 2022	20	16
Temporal cross-validation	2018	32	32
	2019	40	38
	2020	35	32
	2021	50	49
	2022	35	28

22%. Temporal leave-out cross-validation of the GBM model indicated that, for the years 2018, 2020, and 2022, the Root Mean Square Error (RMSE) values nearly doubled, reaching 32 g.m^{-2}, 32 g.m^{-2}, and 28 g.m^{-2}, respectively. In contrast, the years 2019 and 2021 exhibited higher RMSE values, particularly in 2021 (Table 6). A summary of the calibration and validation results is shown in Table 5. The results indicated that the most significant standardization variables, ranked by their importance, included the relative humidity of the air, the soil surface temperature, the solar azimuth, and the photosynthetically active radiation, and they significantly improved millet grain yield estimation, capturing 78% of the variability in validation. Interestingly, the relative humidity of the air was ranked second among the important variables in the machine learning model, just after the most important NDTI. The results (see Fig. 9) of the comparison with Landsat 8 data showed, upon validation, a coefficient of determination ($R^2 = 0.47$), insufficient to ensure the model's robustness compared to the results obtained by UAV with an ($R^2 = 0.78$. This underscores the relevance of utilizing UAV-acquired data to generate a robust model for estimating millet grain yield.

C. MILLET GRAIN YIELD MAP AND YIELD COMPARISON

We used the GBM-based machine learning model to extrapolate millet grain yield from the subplots where the model was calibrated to the whole plot. We constructed millet grain yield maps (Fig. 10) for each field where the ground truth total harvest was conducted. The average error over the four years of harvest was 17.5%. The results exhibit yield variability surrounding the crown of *F. albida*, displaying a gradient that signifies the impact of *F. albida* on pearl millet grain yield. A summary of the comparison between the estimated and measured yields is presented in Table 7. We observed a trend to overestimate yield at the whole-plot scale.

TABLE 7. Comparison (error) between measurements at the whole-plot scale. The relative error was computed as |(Ymeas-Ysim)| / Ysim.

Year	Measured Yield ton grain h^{-1}	Estimated Yield ton grain h^{-1}	Relative Error (%)	Plot Area m^2
2018	0.73	0.80	09	8994
2019	0.36	0.43	16	19685
2020	0.56	0.76	26	11275
2022	0.46	0.57	19	11275

IV. DISCUSSION

The use of UAVs for the intensive monitoring of cultivated fields has led to a very active research area in the real-time prediction of yield based on proxy-sensing data. As a crop that serves as a food source for smallholder farming, pearl millet deserves an accurate prediction of grain yield for mapping crop productivity under complex and heterogeneous environments to adjust practices with precision and anticipation across landscapes and variable climatic years. If proven to be generic, a refined method for data analysis would save tremendous work in the field in the future. We will discuss below whether a generic method can be proposed for pearl millet and under which conditions.

A. THE BEST FLIGHT'S DATE PER YEAR CHANGED WITH THE VARIABILITY IN AGRICULTURAL PRACTICES AND CLIMATIC YEARS

In this part, the relationship between the millet grain yield and NDRE was tested at different stages of crop development. However, the correlation between the yield and NDRE was highly dependent on environmental conditions and on interannual rainfall variability, on stage crop growth and quantity. The results showed that the pre-heading period was usually the best time for predicting millet grain yield. Indeed, this period was characterized by the absence of weeds and leaf senescence, and the effects of agricultural practices were less pronounced than those at the end of the crop cycle. Furthermore, during this period, the vegetation displays substantial greenness, and the millet plants are clearly distinguishable. In contrast, during the harvest period, the millet plants bend significantly due to strong winds accompanying the rains. This clump causes an overlapping effect between the plants, hindering the capture of reflectance from the entire vegetation present on the surface. Similar results have been obtained by [26] and [74] for wheat and rice yield prediction. For 2021 and 2022, the study was conducted on a network of smallholder plots (2021:

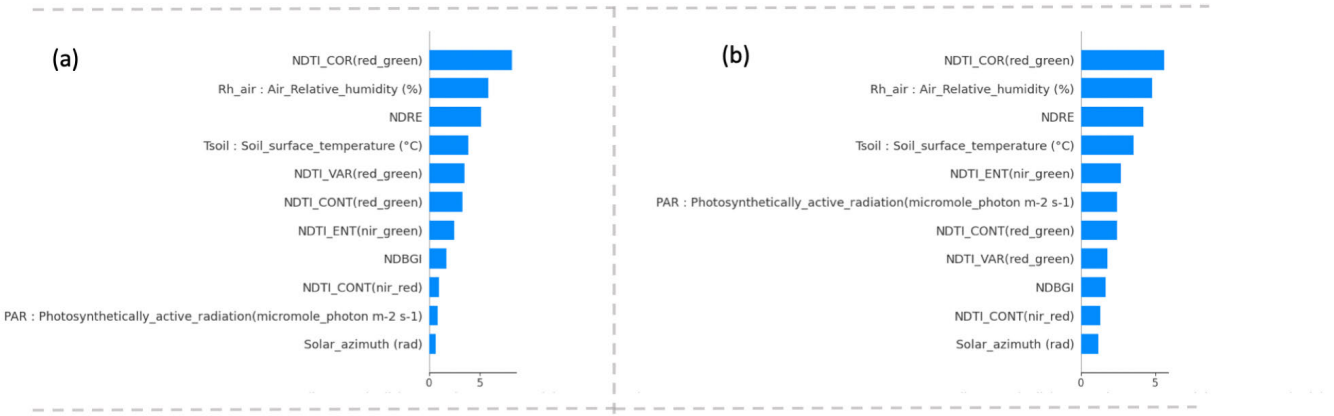

FIGURE 7. Ranking of features importance (Shap value) according to Gradient Boosting Machine (GBM) method (a) and to Random Forest method (based on Out-Of-Bag) (b).

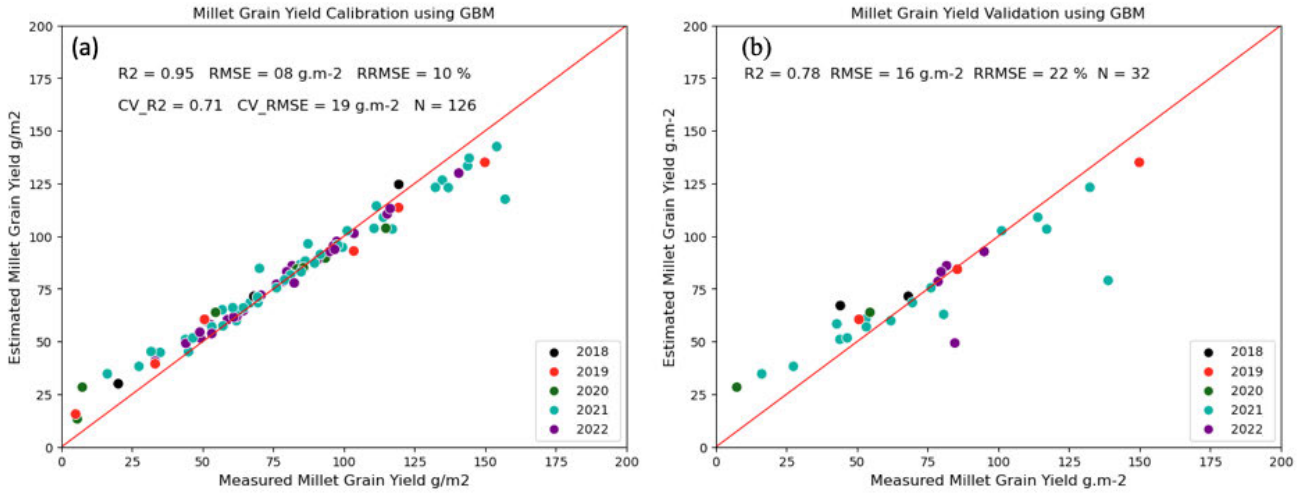

FIGURE 8. Relationship between millet grain yield and combinations of Vis + NDTIs + standardization variables in calibration (a: N = 126 dots) and validation (b: N = 32 dots), using the Gradient Boosting Machine (GBM) method. One dot is one groundtruth subplot of 15 m^2.

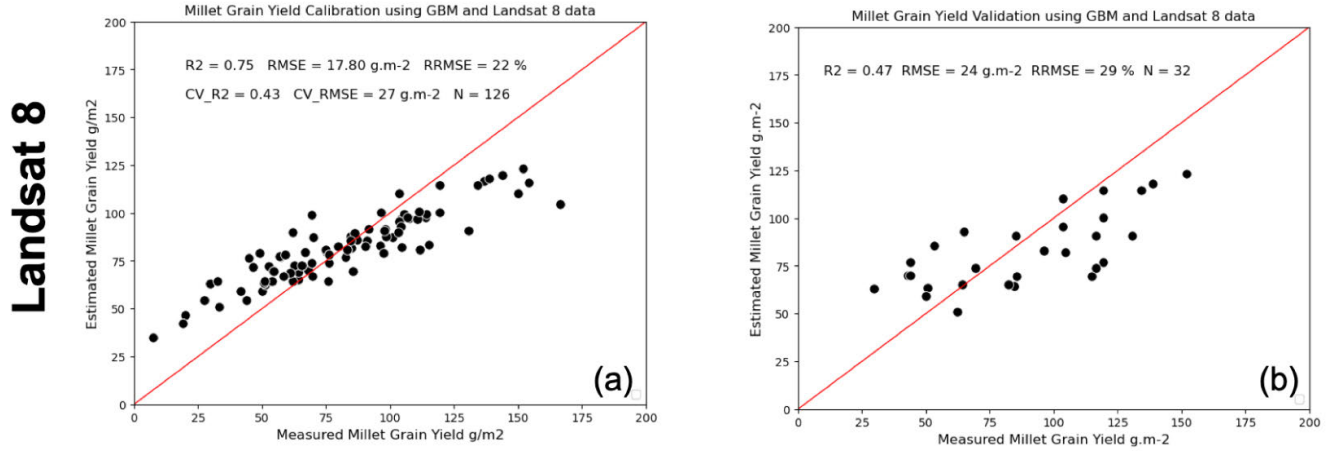

FIGURE 9. Relationship between millet grain yield and GCVI using Landsat 8 data in calibration (a: N = 126 dots) and validation (b: N = 32 dots), using the Gradient Boosting Machine (GBM) method. One dot is one groundtruth subplot of 15 m^2.

8 and 2022: 5), resulting in a similar ranking of dates but with high variability in R^2, likely caused by different agricultural practices and environmental factors. However, the investigation into the correlation between NDRE and

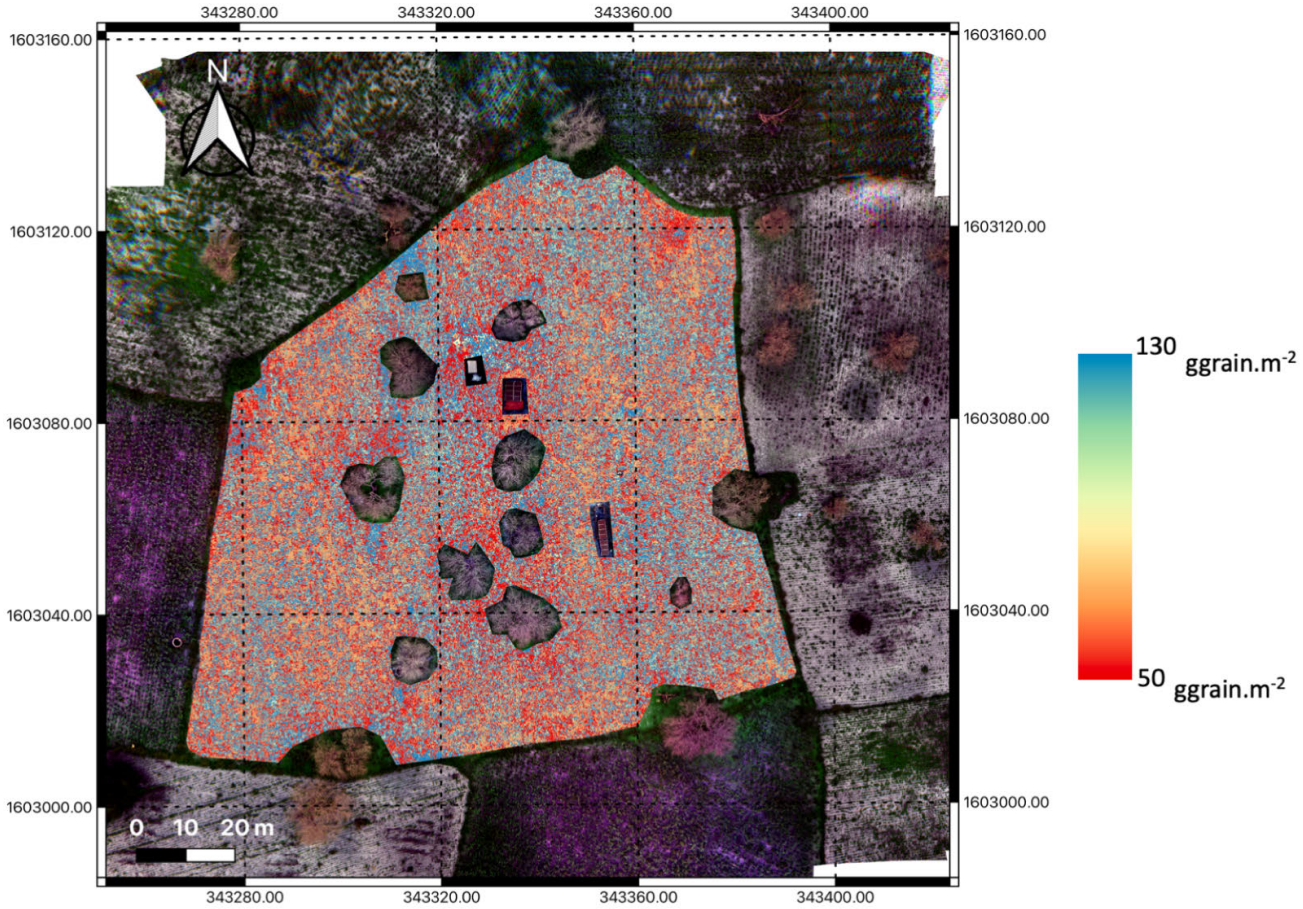

FIGURE 10. Whole-plot maps for one extreme year in terms of rainfall, using the relationship from Fig. 7 (scale is in ggrain.m^{-2}, rainfall = 822 mm).

yield serves primarily to construct our database with the optimal dates, laying the foundation for subsequent in-depth analyses utilizing advanced machine learning techniques. Therefore, we argue that the pre-heading stage can be generally considered the optimal period for estimating millet grain yield based on the results from 2021 and 2022, despite the large residual variability. Therefore, when possible, it is recommended to fly several times during the growing season, with a priority on pre-heading and harvest periods, and to choose the best date *a posteriori*. Moreover, depending on a single vegetation index may introduce uncertainties in determining optimal dates. Thus, we recommend comparing indices that highlight different characteristics of the plant: chlorophyll content index, nitrogen stress index, water stress index, and dry matter stress index.

B. GBM MODEL OUTPERFORMED RANDOM FOREST

In this study, we compared two machine learning methods (GBM and RF) that can be proposed alternatively to predict millet grain yield and illustrate the importance of variables. One of the goals of this study was to upscale millet grain yield from subplots to the whole plot through ML methods. Thus, the results showed that the model based on GBM (gradient boosting machine) provided better calibration performance (Table 5; R^2 = 0.95; RRMSE = 10%) and validation performance (Table 5; R^2 = 0.78; RRMSE = 22%) than the model obtained with RF (random forest) by combining Vis (visible), NDTIs (normalized difference texture index), and standardization variables. The temporal leave-out cross-validation of the GBM model revealed inter-annual variability across different years, given the higher difficulty for the model to predict (validating) the yearly crop, when the observations from this year are absent from the training set. One of the difficulties in this work is the heterogeneity of the data, with a large dataset in 2021 and crop rotation each year (2018, 2019 and 2020, 2021, 2022), that is utilized, explaining the large temporal variability. Although RF and GBM both rely on the use of trees, they differ in their internal construction and evaluation [75]. Furthermore, the optimization parameters for the two models are different. Reference [76] demonstrated the superiority of the GBM model in predicting the prevalence of Listeria spp. in livestock environments compared to RF. Additionally, [77] utilized multiple ML techniques to assess the performance of corn yield estimation and showed that the GBM-based model outperformed the RF-based model. GBM can achieve higher accuracy compared to RF due to optimization parameters that facilitate the correction of mutual errors, and then allowing

it to capture complex patterns in data with high variability. The model derived from UAV data exhibited significantly more substantial results compared to the model based on Landsat 8 data. Indeed, our study is conducted at the intra-plot scale, which requires fine spatial resolution to capture the variability introduced by the presence of trees. The yield data collected were obtained from plots of 15 m^2 (3m x 5m). The pixel size of Landsat data is 15 times larger than the area of the plots used to measure millet grain yield. However, the performance of ML models depends on data structuring, which is why comparing different methods is a valuable alternative to identify the model that best fits the acquisition data. In addition, the constraint on the number of data points significantly impacts the performance of the model, given that machine learning approaches demand abundant data for robust learning. However, we suggest experiments similar to the one conducted in 2021, entailing a reduction in subplot size and a broader distribution within the field. This approach could potentially allow the development of machine learning models on a date-specific basis or through the integration of all phenological dates, facilitating the assessment of interactions between dates and years.

C. THE INTEGRATION OF TEXTURE INDICES AND NORMALIZATION OF REFLECTANCE IMPROVE THE ESTIMATION OF MILLET GRAIN YIELD

Vegetation indices have been widely used to predict crop yield but with certain limitations. Indeed, [78], [79], [80] showed that vegetation indices tended to saturate, especially at advanced phenological stages of the crop, with the onset of senescence, panicles, and weeds. The use of texture increased the dimensionality of UAV image data, which was limited by the number of spectral bands. Texture allowed for the assessment of spatial relationships between neighboring pixel pairs, providing a better description of spatial configuration and crop intensities. It has been reported as a promising technique for precision agriculture using UAV imagery [31]. Both [31] and [34] explored the impact of including texture in modeling crop characteristics. References [78], [81], [82], and [83] demonstrated the potential of texture indices in crop identification and trait estimation. Reference [31] showed significant performance of texture indices compared to vegetation indices in estimating the aboveground biomass of rice. Similarly, [34] reported that the use of texture information alongside spectral and canopy height data improved the prediction accuracy over the VI model in predicting soybean grain yield. Our study confirmed that combining texture indices with vegetation indices (NDTIs) improved millet grain yield prediction. Over 60% of the pearl millet variability was captured in validation using the GBM model including texture indices. Texture attributes offer a more precise description of spatial configurations, color, and intensities in crops. This can be attributed to the sensitivity of texture variables to the structural characteristics of the canopy, while Vegetation Indices (VIs) serve as a proxy for vegetation content. Indeed, normalizing texture properties allowed for a better consideration of variability in canopy architectures and helped to minimize the effects of soil, sun angle, and sensor viewing angle. This is why the millet grain yield estimation was significantly improved by using NDTIs. Analysis of variable importance from the GBM model showed that the correlation-based NDTI, calculated between the red and green bands, ranked first for millet grain yield estimation. Moreover, we used data from the pre-heading stage, characterized by pronounced plant greenness and extensive soil coverage. During this developmental phase, green plants have substantial absorption in the red band and increased reflectance in the green, while the soil exhibits significant reflectance in the red. This phenomenon may elucidate why the correlation-based NDTIs computed using the red and green bands hold greater significance than NDTIs computed using the near-infrared band. Furthermore, the absence of radiometric calibration and flights under different environmental conditions leave noise to the spectral band signal and hence the vegetation indices. In this study, the area was equipped with a standard meteorology station on the flux tower that provides ancillary information related to environmental conditions during the UAV flights. Thus, we selected the best standardization variables obtained from the meteorology station to normalize the reflectance of spectral bands and indirectly the vegetation indices. Combining standardization variables with spectral and texture information proved here to be an alternative to the absence of radiometric correction with carpets. We searched the literature, but to our knowledge, such attempts have not yet been reported. In the future, it might be advisable to test standardization variables directly on radiometrically corrected images.

D. UPSCALING YIELD FROM THE SUBPLOTS TO THE WHOLE-PLOT THROUGH ML METHODS

The satisfactory results obtained with the GBM model allowed us to extrapolate from the plot-level yield to the entire field. The GBM model was built using data from 2018 to 2022, encompassing 16 smallholder plots and 158 subplots. This involved various agricultural practices and therefore a high level of variability. Thus, the model accounted for both intra- and inter-plot variability, as well as interannual variability, yielding satisfactory results even in validation (Fig. 8(b); $R^2 = 0.78$; RRMSE = 22%). In 2020, [35] explored the use of only vegetation indices to predict millet grain yield and obtained a significant but much weaker correlation between yield and MSAVI2 at the time of harvest ($R^2 = 0.47$; RRMSE = 46%). This pioneering study triggered the need to explore more years, plots, textures, standardization and models to determine whether a generic model could be proposed. The 2018 wet season had only 474 mm rainfall, millet grew much better close to the trees, and the positive effect of Faidherbia on millet yields in its neighborhood was visible. Using the same scale, but now in 2022 (rainfall = 822 mm), the millet yield was much higher,

regardless of the distance to the trees, indicating that some drought limitations to productivity have been compensated under abundant rainfall. Furthermore, extrapolating millet grain yield to the whole plot enabled a reasonable comparison between the estimated yield from the model and the yield measured by the farmer at harvest. Comparing our results to those obtained by [35] under the same conditions but with a much simpler method (relative error = 20% between measured and UAV-NDVI estimated yield) for the same field and data collection year (2018) demonstrated a significant improvement and a more robust model in millet grain yield estimation in the whole plot with the refined method proposed here. However, the imprecision stemming from the harvest protocol (relation between the fresh weight of the spikes and the dry weight of the grains) was practical and realistic, yet not accurate, given the potential significant variation in moisture content. This result tells us that part of the 17.5% average accuracy may be due to measurement error in the field. As suggested by [35], we achieved a much more robust millet grain yield estimation by employing a wide range of vegetation indices, normalized texture indices, standardization variables, and machine learning techniques. This yield map will be instrumental for assessing the influence of *F. albida* on pearl millet grain yield through the application of geostatistical methods and semivariogram analysis.

V. CONCLUSION

Our results demonstrated that the whole-plot millet grain yield could be accurately estimated using UAV imagery for different years of cultivation, even in a highly heterogeneous agroforestry park. Here, we proposed a generic method for pearl millet data analysis that provided an accurate estimation of pearl millet yield at both the subplot and the whole-plot scales. Machine learning models, namely, RF and GBM, were utilized to predict millet grain yield by incorporating spectral band information, texture indices, and meteorological standardization variables obtained at the time of flight. The key findings indicated that the including NDTIs showed promise as an alternative to conventional vegetation indices for mapping and predicting millet grain yield with precision. Additionally, standardization variables offered a means of normalizing reflectance values. Such an approach, which was developed in bush agroforestry fields with low levels of productivity (poor soils, deficit of soil organic matter, no fertilizer, reliance on natural rainfall variability), would deserve an extension of its calibration and validation across new landscapes, particularly with conditions close to the potential productivity of millet, such as those encountered in experimental stations, with fertilization, irrigation, and selected varieties. We argue that the methodology proposed here is mature enough also to be applied to other crops (e.g., groundnut) or to other crop associations in the field (e.g., crops grown with other trees or bush species such as *Guiera senegalensis* or *Piliostigma reticulatum* in place of *Faidherbia albida*).

ACKNOWLEDGMENT

The authors would like to thank the M.Sc. students (Marième Faye, Al Housseynou Dabo, and Pape Oumar Ba Bousso) for their help in data acquisition. Among the native people from Sob and Niakhar, they are extremely indebted to Ibou Diouf, Saliou Diouf, and Ngor Diouf. They would also like to express their sincere gratitude to Dr. Georg Cadish (georg.cadisch@uni-hohenheim.de) for his invaluable ideas in standardizing the model through external radiative variables.

REFERENCES

[1] *The State of Food Security and Nutrition in the World 2022*, FAO, Rome, Italy, 2022.
[2] C. Parmesan, M. D. Morecroft, and Y. Trisurat, "Climate change 2022: Impacts, adaptation and vulnerability," Ph.D. dissertation, GIEC, 2022.
[3] *The Sustainable Development Goals Report 2016 | United Nations ILibrary*.
[4] R. DeFries, J. Fanzo, R. Remans, C. Palm, S. Wood, and T. L. Anderman, "Metrics for land-scarce agriculture," *Science*, vol. 349, no. 6245, pp. 238–240, Jul. 2015.
[5] M. Herrero, P. K. Thornton, B. Power, J. R. Bogard, R. Remans, S. Fritz, J. S. Gerber, G. Nelson, L. See, K. Waha, R. A. Watson, P. C. West, L. H. Samberg, J. van de Steeg, E. Stephenson, M. van Wijk, and P. Havlík, "Farming and the geography of nutrient production for human use: A transdisciplinary analysis," *Lancet Planet. Health*, vol. 1, no. 1, pp. e33–e42, Apr. 2017.
[6] P. R. Nair, *An Introduction to Agroforestry*. Cham, Switzerland: Springer, 2021.
[7] C. Mbow, M. Van Noordwijk, E. Luedeling, H. Neufeldt, P. A. Minang, and G. Kowero, "Agroforestry solutions to address food security and climate change challenges in Africa," *Current Opinion Environ. Sustainability*, vol. 6, pp. 61–67, Feb. 2014.
[8] H. N. D. Souza, R. G. M. de Goede, L. Brussaard, I. M. Cardoso, E. M. G. Duarte, R. B. A. Fernandes, L. C. Gomes, and M. M. Pulleman, "Protective shade, tree diversity and soil properties in coffee agroforestry systems in the Atlantic rainforest biome," *Agricult., Ecosystems Environ.*, vol. 146, no. 1, pp. 179–196, Jan. 2012.
[9] P. A. Nyong and N. T. Martin, "Enhancing agricultural sustainability and productivity under changing climate conditions through improved agroforestry practices in smallholder farming systems in sub-saharan Africa," *Afr. J. Agricult. Res.*, vol. 14, no. 7, pp. 379–388, Feb. 2019.
[10] J. Bayala, J. Sanou, H. R. Bazié, R. Coe, A. Kalinganire, and F. L. Sinclair, "Regenerated trees in farmers' fields increase soil carbon across the Sahel," *Agroforestry Syst.*, vol. 94, no. 2, pp. 401–415, Apr. 2020.
[11] S. E. Castle, D. C. Miller, P. J. Ordonez, K. Baylis, and K. Hughes, "The impacts of agroforestry interventions on agricultural productivity, ecosystem services, and human well-being in low- and middle-income countries: A systematic review," *Campbell Systematic Rev.*, vol. 17, no. 2, p. e1167, Jun. 2021.
[12] J. Bayala and I. Prieto, "Water acquisition, sharing and redistribution by roots: Applications to agroforestry systems," *Plant Soil*, vol. 453, nos. 1–2, pp. 17–28, Aug. 2020.
[13] C. Bucagu, B. Vanlauwe, M. T. Van Wijk, and K. E. Giller, "Assessing farmers' interest in agroforestry in two contrasting agro-ecological zones of Rwanda," *Agroforestry Syst.*, vol. 87, no. 1, pp. 141–158, Feb. 2013.
[14] M. A. Altieri, F. R. Funes-Monzote, and P. Petersen, "Agroecologically efficient agricultural systems for smallholder farmers: Contributions to food sovereignty," *Agronomy Sustain. Develop.*, vol. 32, no. 1, pp. 1–13, Jan. 2012.
[15] L. Leroux, N. F. Faye, C. Jahel, G. N. Falconnier, A. A. Diouf, B. Ndao, I. Tiaw, Y. Senghor, G. Kanfany, A. Balde, M. Dieye, N. Sirdey, S. A. Loison, M. Corbeels, F. Baudron, and E. Bouquet, "Exploring the agricultural landscape diversity-food security Nexus: An analysis in two contrasted parklands of central Senegal," *Agricult. Syst.*, vol. 196, Feb. 2022, Art. no. 103312.
[16] A. Sharifi, "Yield prediction with machine learning algorithms and satellite images," *J. Sci. Food Agricult.*, vol. 101, no. 3, pp. 891–896, Feb. 2021. [Online]. Available: https://onlinelibrary.wiley.com/doi/abs/10.1002/jsfa.10696

[17] L. Leroux, G. N. Falconnier, A. A. Diouf, B. Ndao, J. E. Gbodjo, L. Tall, A. A. Balde, C. Clermont-Dauphin, A. Bégué, F. Affholder, and O. Roupsard, "Using remote sensing to assess the effect of trees on millet yield in complex parklands of central Senegal," *Agricult. Syst.*, vol. 184, Sep. 2020, Art. no. 102918.

[18] A. Verger, N. Vigneau, C. Chéron, J.-M. Gilliot, A. Comar, and F. Baret, "Green area index from an unmanned aerial system over wheat and rapeseed crops," *Remote Sens. Environ.*, vol. 152, pp. 654–664, Sep. 2014. [Online]. Available: https://www.sciencedirect.com/science/article/pii/S0034425714002193

[19] N. Amarasingam, A. S. Ashan Salgadoe, K. Powell, L. F. Gonzalez, and S. Natarajan, "A review of UAV platforms, sensors, and applications for monitoring of sugarcane crops," *Remote Sens. Appl., Soc. Environ.*, vol. 26, Apr. 2022, Art. no. 100712.

[20] G. N. Muchiri and S. Kimathi, "A review of applications and potential applications of UAV," in *Proc. Sustain. Res. Innov. Conf.*, 2022, pp. 280–283.

[21] J. Sarron, É. Malézieux, C. A. B. Sané, and É. Faye, "Mango yield mapping at the orchard scale based on tree structure and land cover assessed by UAV," *Remote Sens.*, vol. 10, no. 12, p. 1900, Nov. 2018.

[22] L. Yubin, D. Xiaoling, and Z. Guoliang, "Advances in diagnosis of crop diseases, pests and weeds by UAV remote sensing," *Smart Agriculture*, vol. 1, no. 2, p. 1, 2019.

[23] W. Zhu, E. E. Rezaei, H. Nouri, Z. Sun, J. Li, D. Yu, and S. Siebert, "UAV-based indicators of crop growth are robust for distinct water and nutrient management but vary between crop development phases," *Field Crops Res.*, vol. 284, Aug. 2022, Art. no. 108582.

[24] B. Gano, J. S. B. Dembele, A. Ndour, D. Luquet, G. Beurier, D. Diouf, and A. Audebert, "Using UAV borne, multi-spectral imaging for the field phenotyping of shoot biomass, leaf area index and height of west African sorghum varieties under two contrasted water conditions," *Agronomy*, vol. 11, no. 5, p. 850, Apr. 2021.

[25] L. Pádua, J. Vanko, J. Hruška, T. Adão, J. J. Sousa, E. Peres, and R. Morais, "UAS, sensors, and data processing in agroforestry: A review towards practical applications," *Int. J. Remote Sens.*, vol. 38, nos. 8–10, pp. 2349–2391, May 2017, doi: 10.1080/01431161.2017.1297548.

[26] X. Zhou, H. B. Zheng, X. Q. Xu, J. Y. He, X. K. Ge, X. Yao, T. Cheng, Y. Zhu, W. X. Cao, and Y. C. Tian, "Predicting grain yield in Rice using multi-temporal vegetation indices from UAV-based multispectral and digital imagery," *ISPRS J. Photogramm. Remote Sens.*, vol. 130, pp. 246–255, Aug. 2017.

[27] J. Torres-Sánchez, J. M. Peña, A. I. de Castro, and F. López-Granados, "Multi-temporal mapping of the vegetation fraction in early-season wheat fields using images from UAV," *Comput. Electron. Agricult.*, vol. 103, pp. 104–113, Apr. 2014.

[28] R. Jannoura, K. Brinkmann, D. Uteau, C. Bruns, and R. G. Joergensen, "Monitoring of crop biomass using true colour aerial photographs taken from a remote controlled hexacopter," *Biosyst. Eng.*, vol. 129, pp. 341–351, Jan. 2015.

[29] S. Ninsawat and J. Som-Ard, "Integration of RGB-based vegetation index, crop surface model and object-based image analysis approach for sugarcane yield estimation using unmanned aerial vehicle," *Comput. Electron. Agricult.*, vol. 180, Jan. 2021, Art. no. 105903.

[30] C. Gao, X. Ji, Q. He, Z. Gong, H. Sun, T. Wen, and W. Guo, "Monitoring of wheat fusarium head blight on spectral and textural analysis of UAV multispectral imagery," *Agriculture*, vol. 13, no. 2, p. 293, Jan. 2023.

[31] H. Zheng, T. Cheng, M. Zhou, D. Li, X. Yao, Y. Tian, W. Cao, and Y. Zhu, "Improved estimation of Rice aboveground biomass combining textural and spectral analysis of UAV imagery," *Precis. Agricult.*, vol. 20, no. 3, pp. 611–629, Jun. 2019.

[32] F. Wang, Q. Yi, J. Hu, L. Xie, X. Yao, T. Xu, and J. Zheng, "Combining spectral and textural information in UAV hyperspectral images to estimate Rice grain yield," *Int. J. Appl. Earth Observ. Geoinf.*, vol. 102, Oct. 2021, Art. no. 102397.

[33] S. Li, F. Yuan, S. T. Ata-UI-Karim, H. Zheng, T. Cheng, X. Liu, Y. Tian, Y. Zhu, W. Cao, and Q. Cao, "Combining color indices and textures of UAV-based digital imagery for Rice LAI estimation," *Remote Sens.*, vol. 11, no. 15, p. 1763, Jul. 2019.

[34] T. R. Alabi, A. T. Abebe, G. Chigeza, and K. R. Fowobaje, "Estimation of soybean grain yield from multispectral high-resolution UAV data with machine learning models in west Africa," *Remote Sens. Appl., Soc. Environ.*, vol. 27, Aug. 2022, Art. no. 100782.

[35] O. Roupsard, A. Audebert, A. P. Ndour, C. Clermont-Dauphin, Y. Agbohessou, J. Sanou, J. Koala, E. Faye, D. Sambakhe, C. Jourdan, G. le Maire, L. Tall, D. Sanogo, J. Seghieri, L. Cournac, and L. Leroux, "How far does the tree affect the crop in agroforestry? New spatial analysis methods in a faidherbia parkland," *Agricult., Ecosyst. Environ.*, vol. 296, Jul. 2020, Art. no. 106928.

[36] R. Lalou, B. Sultan, B. Müller, and A. Ndonky, "Does climate opportunity facilitate smallholder farmers' adaptive capacity in the sahel?" *Palgrave Commun.*, vol. 5, no. 1, pp. 1–11, Jul. 2019.

[37] D. M. L. Diongue, O. Roupsard, F. C. Do, C. Stumpp, D. Orange, S. Sow, C. Jourdan, and S. Faye, "Evaluation of parameterisation approaches for estimating soil hydraulic parameters with HYDRUS-1D in the groundnut basin of Senegal," *Hydrolog. Sci. J.*, vol. 67, no. 15, pp. 2327–2343, Nov. 2022.

[38] M. Niang, B. Seydi, and I. Hathie, "Etude de la consommation des céréales de base au Sénégal," *Feed Future Naatal Mbay-USAID*, p. 128, 2017.

[39] C. T. Satyavathi, S. Ambawat, V. Khandelwal, and R. K. Srivastava, "Pearl millet: A climate-resilient nutricereal for mitigating hidden hunger and provide nutritional security," *Frontiers Plant Sci.*, vol. 12, Sep. 2021.

[40] M. Debieu, G. Kanfany, and L. Laplaze, "Pearl millet genome: Lessons from a tough crop," *Trends Plant Sci.*, vol. 22, no. 11, pp. 911–913, Nov. 2017.

[41] *Flying Eye—Drone Professionnel, Accessoires, Formation*.

[42] *Hiphen—Plant Phenotyping Crop Image Analytics Solutions*.

[43] *P4 Multispectral—Specifications—DJI*.

[44] *Metashape Python Reference*.

[45] R. Bivand, T. Keitt, B. Rowlingson, E. Pebesma, M. Sumner, R. Hijmans, E. Rouault, and M. R. Bivand, "Package 'Rgdal,'" Tech. Rep., 2015, p. 172.

[46] R. J. Hijmans, J. Van Etten, J. Cheng, M. Mattiuzzi, M. Sumner, J. A. Greenberg, O. P. Lamigueiro, A. Bevan, E. B. Racine, and A. Shortridge, "Package 'Raster," Rep., 2015, vol. 734, p. 473.

[47] *R for MacOS*.

[48] J. W. Rouse, R. H. Haas, J. A. Schell, and D. W. Deering, "Monitoring vegetation systems in the great plains with ERTS," Tech. Rep., vol. 351, no. 1, p. 309.

[49] A. A. Gitelson, Y. Gritz, and M. N. Merzlyak, "Relationships between leaf chlorophyll content and spectral reflectance and algorithms for non-destructive chlorophyll assessment in higher plant leaves," *J. Plant Physiol.*, vol. 160, no. 3, pp. 271–282, Jan. 2003.

[50] C. J. Tucker, "Red and photographic infrared linear combinations for monitoring vegetation," *Remote Sens. Environ.*, vol. 8, no. 2, pp. 127–150, May 1979.

[51] A. Gitelson and M. N. Merzlyak, "Spectral reflectance changes associated with autumn senescence of *Aesculus hippocastanum* L. and *Acer platanoides* L. Leaves. spectral features and relation to chlorophyll estimation," *J. Plant Physiol.*, vol. 143, no. 3, pp. 286–292, Mar. 1994.

[52] C. F. Jordan, "Derivation of leaf-area index from quality of light on the forest floor," *Ecology*, vol. 50, no. 4, pp. 663–666, Jul. 1969.

[53] A. A. Gitelson, Y. J. Kaufman, and M. N. Merzlyak, "Use of a green channel in remote sensing of global vegetation from EOS-MODIS," *Remote Sens. Environ.*, vol. 58, no. 3, pp. 289–298, Dec. 1996.

[54] A. R. Huete, "A soil-adjusted vegetation index (SAVI)," *Remote Sens. Environ.*, vol. 25, no. 3, pp. 295–309, Aug. 1988.

[55] C. R. Perry and L. F. Lautenschlager, "Functional equivalence of spectral vegetation indices," *Remote Sens. Environ.*, vol. 14, nos. 1–3, pp. 169–182, Jan. 1984.

[56] G. Rondeaux, M. Steven, and F. Baret, "Optimization of soil-adjusted vegetation indices," *Remote Sens. Environ.*, vol. 55, no. 2, pp. 95–107, Feb. 1996.

[57] J. Bendig, K. Yu, H. Aasen, A. Bolten, S. Bennertz, J. Broscheit, M. L. Gnyp, and G. Bareth, "Combining UAV-based plant height from crop surface models, visible, and near infrared vegetation indices for biomass monitoring in barley," *Int. J. Appl. Earth Observ. Geoinf.*, vol. 39, pp. 79–87, Jul. 2015.

[58] M. Louhaichi, M. M. Borman, and D. E. Johnson, "Spatially located platform and aerial photography for documentation of grazing impacts on wheat," *Geocarto Int.*, vol. 16, no. 1, pp. 65–70, Mar. 2001.

[59] G. E. Meyer and J. C. Neto, "Verification of color vegetation indices for automated crop imaging applications," *Comput. Electron. Agricult.*, vol. 63, no. 2, pp. 282–293, Oct. 2008.

[60] M. Bossoukpe, E. Faye, O. Ndiaye, S. Diatta, O. Diatta, A. A. Diouf, M. Dendoncker, M. H. Assouma, and S. Taugourdeau, "Low-cost drones help measure tree characteristics in the Sahelian savanna," *J. Arid Environ.*, vol. 187, Apr. 2021, Art. no. 104449.

[61] S. Shimada, J. Matsumoto, A. Sekiyama, B. Aosier, and M. Yokohana, "A new spectral index to detect poaceae grass abundance in Mongolian grasslands," *Adv. Space Res.*, vol. 50, no. 9, pp. 1266–1273, Nov. 2012.

[62] R. Escadafal and A. Huete, "Etude des proprit spectrales des sols arides applique l'amlioration des indices de vgtation obtenus par tldtection," vol. 312, no. 11, pp. 1385–1391, 1991.

[63] D. M. Woebbecke, G. E. Meyer, K. Von Bargen, and D. A. Mortensen, "Color indices for weed identification under various soil, residue, and lighting conditions," *Trans. ASAE*, vol. 38, no. 1, pp. 259–269, 1995.

[64] A. Bannari, D. Morin, F. Bonn, and A. R. Huete, "A review of vegetation indices," *Remote Sens. Rev.*, vol. 13, no. 1, pp. 95–120, 1995.

[65] A. A. Gitelson, Y. J. Kaufman, R. Stark, and D. Rundquist, "Novel algorithms for remote estimation of vegetation fraction," *Remote Sens. Environ.*, vol. 80, no. 1, pp. 76–87, Apr. 2002.

[66] R. M. Haralick, K. Shanmugam, and I. Dinstein, "Textural features for image classification," *IEEE Trans. Syst., Man, Cybern.*, vol. SMC-3, no. 6, pp. 610–621, Nov. 1973.

[67] A. Zvoleff, "GLCM: Calculate textures from grey-level co-occurrence matrices (GLCMs). R package version 1.6.1," Tech. Rep., 2020.

[68] D. L. Whaley III, "The interquartile range: Theory and estimation," Tech. Rep., 2005.

[69] H. P. Vinutha, B. Poornima, and B. M. Sagar, "Detection of outliers using interquartile range technique from intrusion dataset," in *Proc. FICTA*. Cham, Switzerland: Springer, 2018, pp. 511–518.

[70] M. Kuhn, J. Wing, S. Weston, A. Williams, C. Keefer, A. Engelhardt, T. Cooper, Z. Mayer, and B. Kenkel, "Caret: Classification and regression training. Version 6.0–86," Tech. Rep., 2015.

[71] I. Diack, S. M. Diene, L. Louise, D. A. Aziz, H. Benjamin, R. Olivier, L. Philippe, A. Alain, S. Idrissa, and D. Moussa, "Combining UAV and Sentinel-2 imagery for estimating millet FCover in a heterogeneous agricultural landscape of Senegal," *IEEE J. Sel. Topics Appl. Earth Observ. Remote Sens.*, vol. 17, pp. 7305–7322, 2024.

[72] C. G. Thompson, R. S. Kim, A. M. Aloe, and B. J. Becker, "Extracting the variance inflation factor and other multicollinearity diagnostics (don't short) from typical regression results," *Basic Appl. Social Psychol.*, vol. 39, no. 2, pp. 81–90, Mar. 2017.

[73] I. Cohen, Y. Huang, J. Chen, J. Benesty, J. Benesty, J. Chen, Y. Huang, and I. Cohen, "Pearson correlation coefficient," in *Noise Reduction in Speech Processing*. Cham, Switzerland: Springer, 2009, pp. 1–4.

[74] H. Midi and A. Bagheri, "Robust multicollinearity diagnostic measure in collinear data set," in *Proc. 4th Int. Conf. Appl. Math., Simulation, Modeling*, 2010, pp. 138–142.

[75] A. Liaw and M. Wiener, "Classification and regression by randomForest," *R News*, vol. 2, no. 3, pp. 18–22, 2002.

[76] C. E. Golden, M. J. Rothrock, and A. Mishra, "Comparison between random forest and gradient boosting machine methods for predicting listeria spp. Prevalence in the environment of pastured poultry farms," *Food Res. Int.*, vol. 122, pp. 47–55, Aug. 2019.

[77] F. Babaie Sarijaloo, M. Porta, B. Taslimi, and P. M. Pardalos, "Yield performance estimation of corn hybrids using machine learning algorithms," *Artif. Intell. Agricult.*, vol. 5, pp. 82–89, 2021.

[78] J. L. Hatfield, A. A. Gitelson, J. S. Schepers, and C. L. Walthall, "Application of spectral remote sensing for agronomic decisions," *Agronomy J.*, vol. 100, no. S3, p. 117, May 2008.

[79] P. S. Thenkabail, R. B. Smith, and E. De Pauw, "Hyperspectral vegetation indices and their relationships with agricultural crop characteristics," *Remote Sens. Environ.*, vol. 71, no. 2, pp. 158–182, Feb. 2000.

[80] A. C. Kedia, B. Kapos, S. Liao, J. Draper, J. Eddinger, C. Updike, and A. E. Frazier, "An integrated spectral–structural workflow for invasive vegetation mapping in an arid region using drones," *Drones*, vol. 5, no. 1, p. 19, Mar. 2021.

[81] J. E. Böhler, M. E. Schaepman, and M. Kneubühler, "Crop classification in a heterogeneous arable landscape using uncalibrated UAV data," *Remote Sens.*, vol. 10, no. 8, p. 1282, Aug. 2018.

[82] *Gray Level co-Occurrence Matrix (GLCM) Texture Based Crop Classification Using Low Altitude Remote Sensing Platforms [PeerJ].*

[83] G.-H. Kwak and N.-W. Park, "Impact of texture information on crop classification with machine learning and UAV images," *Appl. Sci.*, vol. 9, no. 4, p. 643, Feb. 2019.

SERIGNE MANSOUR DIENE received the degree in engineering surveying. He is currently pursuing the Ph.D. degree in computer science specializing in remote sensing applied to agriculture with the Computer Science Department, Cheikh Anta Diop University (UCAD), in collaboration with French agricultural research and international cooperation organization (CIRAD). As part of his research work, he is posted at the LMI IESOL (IRD-UCAD-ISRA) and works on estimating crop yields in agroforestry systems and the spatialized assessment of the effect of trees on crops using aerial imagery obtained by UAV and statistical approaches. In addition, he obtained his degree by working on sorghum phenotyping for varietal creation programs using thermal images from UAV to assess the crop's level of water stress.

IBRAHIMA DIACK received the master's degree in marine ecology. He is currently pursuing the Ph.D. degree with the Mathematic and Informatic Department, Cheikh Anta Diop University, Dakar, Senegal, in collaboration with French agricultural research and International Cooperation Organization (CIRAD) and the Centre de Suivie Ecologique (CSE), Senegal. He has worked with different kinds of oceanographic and atmospheric data from remote sensing (Ocena color, Ascat, and QuikSCAT) and oceanographic in-situ data (CTD, acoustic, and nutrients). He is also a Senegal citizen. He works mainly on the development of crop monitoring solutions using UAV and satellite combination together with empirical approaches.

ALAIN AUDEBERT is currently a French Senior Scientist at CIRAD (Agricultural Research for Development: http://www.cirad.fr/en). His area of expertise is ecophysiology for a better understanding of adapting tropical crops to abiotic constraints. For several years now, his field of activity has been focused on high-throughput phenotyping methods, notably using UAV onboard imagery.

OLIVIER ROUPSARD is currently a French Senior Scientist at CIRAD (Agricultural Research for Development: http://www.cirad.fr/en). He focuses on tropical agroforestry, bioclimatology, and modeling, with some interest also in hydrology and proxy-sensing as well. He has been a Principal Investigator (PI) of several FLUXNET eddy-covariance sites in the tropics. He is currently posted in Senegal to work on Sahelian agro-salvo-pastoral systems (*Faidherbia-Flux*: https://lped.info/wikiObsSN/?Faidherbia-Flux).

LOUISE LEROUX is currently a Researcher with CIRAD, AIDA Unit, Montpellier, France, which works on agroecology and sustainable intensification of annual crop production in terms of quantity and also quality where it is relevant, in a particularly constrained tropical environment. She is also a Geographer with a strong background in remote sensing applied to agricultural monitoring. She focuses her research on the use of remote sensing technologies combined with statistical or biophysical modeling to improve the cropping systems descriptions (where are the crop areas and what kind of crops, what are the agricultural practices, what are the interactions with the surrounding landscape? etc.) and improve the assessment of agronomical and environmental performances of smallholder cropping systems. Over the last few years, she worked mainly in West Africa, with a focus on agroforestry systems. She was previously seconded to Centre de Suivi Ecologique, Dakar, Senegal, and she is currently with IITA, Nairobi, Kenya, where she conducts her research mainly in Ethiopia and Rwanda.

ABDOUL AZIZ DIOUF received the Ph.D. degree in environmental sciences and management from the University of Liège, Belgium. He is currently with the Centre de Suivi Ecologique (CSE), Dakar, Senegal, as a Research Scientist and a Coordinator of the research and development program. He is also a Researcher of the Pastoralism and Drylands Pole (PPZS) in West Africa. His key activities are 1) acquisition, processing, and analysis of drone and temporal series of satellite images; 2) statistical modeling of forage biomass production and crop yields using earth observation data; and 3) landscape ecology and mapping of natural ecosystem variables.

MODOU MBAYE is currently a Senior Researcher working on artificial intelligence with Drones/Satellites for digital agriculture and environmental applications. He has a long experience in using geospatial technologies and integrating machine learning algorithms and cloud computing technologies. In addition, he was an International Consultant for the IAEA Vienna Austria and the NASA Program SERVIR (connected Space to Village). He supports international organizations by proposing solutions based on satellite data from West African countries. His area of research combines advanced remote sensing with machine learning and deep learning computer vision for geospatial big data applications, such as high-throughput image-based plant phenotyping, UAV-based imaging platforms for precision agriculture, crop classification, crop growth, and yield prediction using Earth observation, multi-source remote sensing, and AI computer vision for instance segmentation.

ROMAIN FERNANDEZ is currently a Computer Science Researcher at CIRAD, Montpellier, France (http://www.cirad.fr/en), where he specializes in developing 2D, 3D, and time-lapse image analysis methods for plant science and sustainable agronomy, particularly in the context of southern countries. His work spans various observational scales from cellular to field levels, with a strong emphasis on integrating interdisciplinary insights and domain knowledge into data modeling. His primary contributions lie in advancing their fundamental understanding of plant systems and automating trait identification and quantification for refining growth models to inform and improve cropping practices under diverse agro-climatic conditions.

MOUSSA DIALLO received the master's degree in electronics and telecommunications from the University of Limoges, France, in 2007, and the Ph.D. degree in telecommunications from the University of Rennes, France. He is currently a Full Professor with the Polytechnic Institute, Cheikh Anta Diop University, Senegal. His research interests include wireless communication, the IoT, and wireless sensor networks.

IDRISSA SARR received the master's degree in computer science from Cheikh Anta Diop University (UCAD), in 2006, and the Ph.D. degree in large-scale distributed databases from Université Pierre et Marie Curie, France, in 2010. From 2011 and 2012, he was a Postdoctoral Researcher in social data analysis with Université du Québec en Outaouais, Canada. He is currently a Teacher-Researcher at UCAD. He is working on data science and artificial intelligence.